KINEMATICS MODELING OF THE ABB7600 ROBOT

Sandra-Elena NICHIFOR[1], Ion STROE[2]

The purpose of this paper is to provide a kinematics model of an ABB IRB7600 robotic arm. Regarding the direct kinematic problem, this is solved using Denavit-Hartenberg parameters. Moreover, the inverse kinematics problem is based on the known iterative methods, respectively the general problem of inverse kinematics and the geometric approach of the position to determine the joints.

The developed kinematics model plays an essential role in enabling the trajectory planning for the ABB 7600 robot. By employing a fourth-order interpolation method, the motion planning process is enhanced, allowing the robot to execute precise and efficient movements along its trajectory.

Keywords: Denavit-Hartenberg parameters, direct kinematics, inverse kinematics, trajectory planning, ABB7600 joints.

1. Introduction

Modeling and simulation are two processes used to develop and test the behavior of a robot in its workspace, which is characterized by the total volume generated by the end effector as the manipulator performs all possible movements. The problem in position control is to control the manipulator end effector (i.e. the joint variables) to the desired position regardless of the initial position [1]. In this sense, the solution will be done in several steps: route planning, trajectory generation and control design.

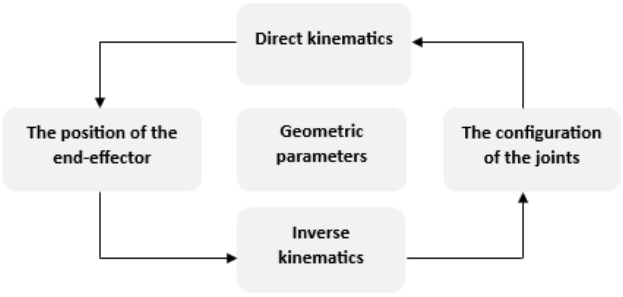

Fig. 1 The relationship between direct kinematics and inverse kinematics

[1] Eng., PhD student, Faculty of Biotechnical Systems Engineering, , National University of Science and Technology POLITEHNICA Bucharest, e-mail: sandra.nichifor@stud.aero.upb.ro (corresponding author)
[2] Prof., Department of Mechanics, National University of Science and Technology POLITEHNICA Bucharest, Romania, e-mail: ion.stroe@gmail.com

The problem of direct kinematics represents the set of all relationships that allow defining the position of the end effector according to the variables of the joints. In this sense, several possibilities for determining the position of the end effector using Cartesian coordinates, cylindrical coordinates, spherical coordinates and articulated coordinates were formulated. Instead, the inverse kinematics problem ensures the determination of the coordinates of the joints that lead the end effector to the desired position and orientation [2].

The main objectives of this paper include developing a kinematics model of an ABB7600 robotic arm using Denavit-Hartenberg parameters to solve the direct kinematics problem. Moreover, solving the inverse kinematics problem by employing iterative methods, such as the general problem of inverse kinematics and a geometric approach is considered.

The originality of this paper aims to contribute to the understanding and control of the ABB7600 robotic arm by providing a comprehensive self-developed model that encompasses kinematics and trajectory planning aspects.

2. Direct kinematics

The direct kinematics problem considers determining the position and orientation of the end effector using the values of the manipulator joints [3],[4].

The transformation matrix for a link ***i*** is

$$[T_i]=\begin{bmatrix} \cos\theta_i & -\sin\theta_i\cos\alpha_i & \sin\theta_i\sin\alpha_i & a_i\cos\theta_i \\ \sin\theta_i & \cos\theta_i\cos\alpha_i & -\cos\theta_i\sin\alpha_i & a_i\sin\theta_i \\ 0 & \sin\alpha_i & \cos\alpha_i & d_i \\ 0 & 0 & 0 & 1 \end{bmatrix} \tag{1}$$

where d_i is the distance between the x_i and x_{i+1} axes along the z_{i+1} axis (represents the extension or retraction of the joint axes), θ_i is the angle between the x_i and x_{i+1} axes, measured about the z_{i+1} axis (represents the rotation about the joint axis), a_i is the distance between the z_i and z_{i+1} axes along the x_i axis (represents the distance between the joint axes) and α_i is the angle between the z_i and z_{i+1} axes, measured about the x_i axis (represents the relative twist between consecutive links) [5].

Regarding the calculation of homogeneous transformation matrices, the following table with Denavit-Hartenberg parameters is used [6]

Table 1

Denavit – Hartenberg parameters of the mechanism

Link	$d_i\,[m]$	$\theta_i\,[\deg]$	$a_i\,[m]$	$\alpha_i[\deg]$
1	0.78	θ_1	0.41	–90
2	0	θ_2	1.075	0
3	0	θ_3	0.165	–90
4	1.056	θ_4	0	90
5	0	θ_5	0	–90
6	0.25	θ_6	0	0

Given that

$$[T]_6^0 = [T]_1^0 [T]_2^1 [T]_3^2 [T]_4^3 [T]_5^4 [T]_6^5 = \begin{bmatrix} [R]_6^0 & P_6^0 \\ 0 & 1 \end{bmatrix} \tag{2}$$

the orientation and position of the final effector of the robot will be obtained

$$[R]_6^0 = \begin{bmatrix} r_{11} & r_{12} & r_{13} \\ r_{21} & r_{22} & r_{23} \\ r_{31} & r_{32} & r_{33} \end{bmatrix} \tag{3}$$

where

$r_{11} = c_1c_{23}c_4c_5c_6 + c_5s_1s_4c_6 - c_1s_{23}s_5c_6 + s_1c_4s_6 - c_1c_{23}s_4s_6$

$r_{12} = s_1c_4c_6 - c_1c_{23}s_4c_6 - c_1c_{23}c_4c_5s_6 - c_5s_1s_4s_6 + c_1s_{23}s_5s_6$

$r_{13} = c_1s_{23}c_5 - c_{23}c_4c_1s_5 - s_1s_4s_5$

$r_{21} = s_1c_{23}c_4c_5c_6 - c_5c_1s_4c_6 - s_1s_{23}s_5c_6 - c_1c_4s_6 - s_1c_{23}s_4s_6$

$r_{22} = -c_1c_4c_6 - s_1c_{23}s_4c_6 - s_1c_{23}c_4c_5s_6 + c_5c_1s_4s_6 + s_1s_{23}s_5s_6$

$r_{23} = s_1s_{23}c_5 - c_{23}c_4s_1s_5 + c_1s_4s_5$

$r_{31} = -s_{23}c_4c_5c_6 - c_{23}s_5c_6 + s_{23}s_4s_6$

$r_{32} = s_{23}s_4c_6 + c_4c_5s_{23}s_6 + c_{23}s_5s_6$

$r_{33} = c_{23}c_5 + c_4s_{23}s_5$

$$P_6^0 = \begin{bmatrix} c_1(a_1 + a_2c_2 + a_3c_{23} - d_4s_{23} - d_6c_5s_{23} - d_6c_{23}c_4s_5) - d_6s_1s_4s_5 \\ s_1(a_1 + a_2c_2 + a_3c_{23} - d_4s_{23} - d_6c_5s_{23} - d_6c_{23}c_4s_5) + d_6c_1s_4s_5 \\ d_1 - a_2s_2 - a_3s_{23} - d_4c_{23} - d_6c_5c_{23} + d_6s_{23}c_4s_5 \end{bmatrix} \quad (4)$$

in which the following notations were made

$$\begin{aligned} s_i &= \sin\theta_i \\ c_i &= \cos\theta_i \\ s_{ij} &= \sin(\theta_i + \theta_j) \\ c_{ij} &= \cos(\theta_i + \theta_j) \end{aligned}, i = j = \overline{1,6} \quad (5)$$

3. Inverse kinematics

In robotics, determining the joint angles of a serial manipulator to locate the position and orientation of the end effector is known as inverse kinematics. Also, solving this inverse kinematics problem is essential for all pick-and-place operations. Although this whole process can be complex, the most efficient way to determine the configurations of all the joints is to define a closed-form expression of the manipulator. In this sense, there are types of manipulators whose closed-form expressions cannot exist, so that numerical methods must be implemented to obtain an inverse kinematic solution, these iterative processes with progressive approximation requiring high computational efforts [7-9].

The forward kinematics model of the ABB7600 robot can be easily derived using the Denavit-Hartenberg model and it can be represented as follows

$$[T]_6^0 = [T]_1^0[T]_2^1[T]_3^2[T]_4^3[T]_5^4[T]_6^5 = [H] \quad (6)$$

with

$$[H] = \begin{bmatrix} h_{11} & h_{12} & h_{13} & P_x \\ h_{21} & h_{22} & h_{23} & P_y \\ h_{31} & h_{32} & h_{33} & P_z \\ 0 & 0 & 0 & 1 \end{bmatrix} \quad (7)$$

where $h_{ij}(i = j = \overline{1,3})$ denotes the components of the rotation matrix of the final effector (are similar to the components of the rotation matrix in relation (3)) and P_x, P_y, P_z represent the final effector position components on the three axes.

Using the (6) and (7) relations is obtained a system of 12 nonlinear equations with 6 unknowns and to determine all the joints, successive multiplication with the inverse matrix of a certain transformation in both sides of

the robot's kinematic equation is considered. Using this method four joints are obtained, respectively

$$\theta_1 = arctg\left(\frac{P_y - d_6 h_{23}}{P_x - d_6 h_{13}}\right) \tag{8}$$

$$\theta_4 = arctg\left(\frac{h_{13}s_1 - h_{23}c_1}{(h_{13}c_1 + h_{23}s_1)c_{23} - h_{33}s_{23}}\right) \tag{9}$$

$$\theta_5 = arctg\left(\frac{(h_{13}c_1 + h_{23}s_1)c_{23}c_4 - h_{33}s_{23}c_4 + (h_{13}s_1 - h_{23}c_1)s_4}{(h_{13}c_1 + h_{23}s_1)s_{23} + h_{33}c_{23}}\right) \tag{10}$$

$$\theta_6 = arctg\left(\frac{-(h_{11}c_1 + h_{21}s_1)c_{23}s_4 + h_{31}s_{23}s_4 + (h_{11}s_1 - h_{21}c_1)c_4}{-(h_{12}c_1 + h_{22}s_1)c_{23}s_4 + h_{32}s_{23}s_4 + (h_{12}s_1 - h_{22}c_1)c_4}\right) \tag{11}$$

Considering the complex mathematical calculation regarding the determination of the angles θ_2 and θ_3, the geometrical problem for the calculation of the two angles will be addressed next. A simple method to solve the inverse kinematics is by removing the last links and keeping the first three joints of the robotic arm to determine the values of the angles θ_2 and θ_3.

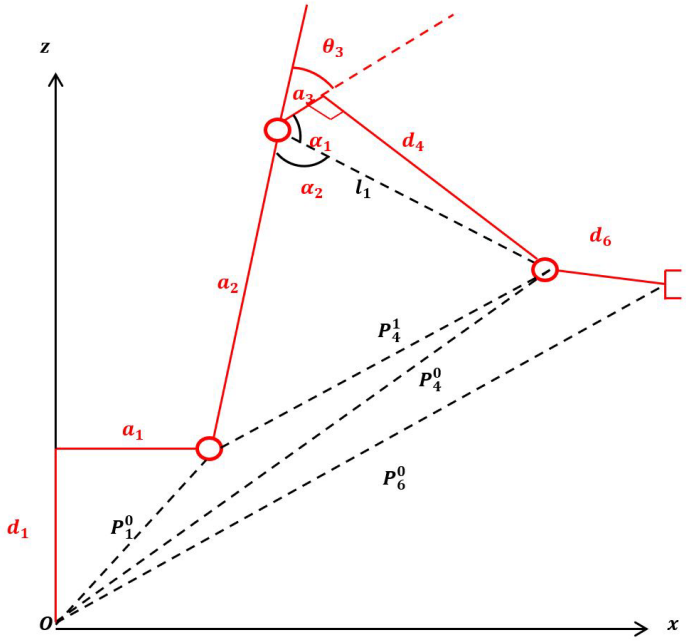

Fig. 2 Simplified side view of the robotic arm

As seen in Fig.2, certain lengths can be determined using trigonometric relations and the Pythagorean theorem in the highlighted right triangles, considering that z represents the position of the end effector on the z axis, respectively P_z, and

$$l_1 = \sqrt{a_3^2 + d_4^2} \tag{12}$$

$$\alpha_1 = arctg\left(\frac{d_4}{a_3}\right) \tag{13}$$

$$\overrightarrow{P_4^1} = \overrightarrow{P_4^0} - \overrightarrow{P_1^0} \tag{14}$$

Relation (14) P_4^0 represents the position of joint four relative to the base of the robotic arm, P_1^0 represents the position of joint one relative to the base of the robotic arm, and P_4^1 represents the position of joint four relative to the first joint.

The position of the first joint relative to the base of the robot is

$$\left\{P_1^0\right\} = \begin{Bmatrix} a_1\cos\theta_1 \\ a_1\sin\theta_1 \\ d_1 \end{Bmatrix} \tag{15}$$

From the above figure it is also observed that

$$\overrightarrow{P_6^0} = \overrightarrow{P_4^0} + \overrightarrow{P_4^6} \tag{16}$$

Given that

$$\left\{P_4^0\right\} = \begin{Bmatrix} P_x \\ P_y \\ P_z \end{Bmatrix} - d_6 \begin{Bmatrix} h_{13} \\ h_{23} \\ h_{33} \end{Bmatrix} \tag{17}$$

is obtained

$$\left\{P_4^1\right\} = \begin{Bmatrix} P_x - d_6h_{13} \\ P_y - d_6h_{23} \\ P_z - d_6h_{33} \end{Bmatrix} - \begin{Bmatrix} a_1\cos\theta_1 \\ a_1\sin\theta_1 \\ d_1 \end{Bmatrix} \tag{18}$$

P_{14} denotes the length of the vector $\overrightarrow{P_4^1}$

$$P_{14} = \sqrt{(P_x - d_6h_{13} - a_1\cos\theta_1)^2 + (P_y - d_6h_{23} - a_1\sin\theta_1)^2 + (P_z - d_6h_{33} - d_1)^2} \tag{19}$$

From Fig. 2 applying the cosine theorem yields

$$\alpha_2 = \arccos\left(\frac{a_2^2 + l_1^2 - P_{14}^2}{2a_2 l_1}\right) \tag{20}$$

Noting on the drawing that $\pi = \theta_3 + \alpha_1 + \alpha_2$, the value of the angle of the third joint is obtained

$$\theta_3 = \pi - arctg\left(\frac{d_4}{a_3}\right) - \arccos\left(\frac{a_2^2 + l_1^2 - P_{14}^2}{2a_2 l_1}\right) \tag{21}$$

Regarding the determination of the angle of the second joint, the geometric elements in the Fig. 3 will be identified

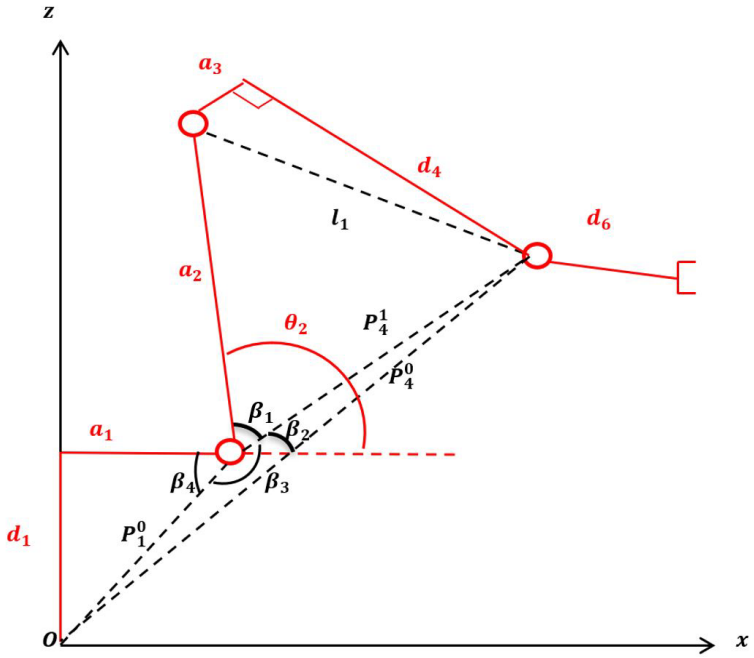

Fig. 3 Lateral view robotic arm

$$\beta_4 = arctg\left(\frac{d_1}{a_1}\right) \tag{22}$$

$$\beta_3 = \pi - \beta_4 = \pi - arctg\left(\frac{d_1}{a_1}\right) \tag{23}$$

The lengths corresponding to the positions of joints two and four relative to the position of the first joint of the robotic arm are

$$P_{01} = \sqrt{(a_1 \cos\theta_1)^2 + (a_1 \sin\theta_1)^2 + d_1^2} \tag{24}$$

$$P_{04} = \sqrt{(P_x - d_6 h_{13})^2 + (P_y - d_6 h_{23})^2 + (P_z - d_6 h_{33})^2} \tag{25}$$

$$\beta_2 + \beta_3 = \arccos\left(\frac{P_{01}^2 + P_{14}^2 - P_{04}^2}{2P_{01}P_{14}}\right) \tag{26}$$

Given that the angle β_3 was defined using the relation (22), it is obtained

$$\beta_2 = \arccos\left(\frac{P_{01}^2 + P_{14}^2 - P_{04}^2}{2P_{01}P_{14}}\right) - \pi + arctg\left(\frac{d_1}{a_1}\right) \tag{27}$$

Applying the cosine theorem

$$\beta_1 = \arccos\left(\frac{a_2^2 + P_{14}^2 - l_1^2}{2a_2P_{14}}\right) \tag{28}$$

The expression of the angle of the second joint is finally obtained, knowing that $\theta_2 = -(\beta_1 + \beta_2)$

$$\theta_2 = \pi - \arccos\left(\frac{a_2^2 + P_{14}^2 - l_1^2}{2a_2P_{14}}\right) - \arccos\left(\frac{P_{01}^2 + P_{14}^2 - P_{04}^2}{2P_{01}P_{14}}\right) - arctg\left(\frac{d_1}{a_1}\right) \tag{29}$$

4. Trajectory planning of a serial manipulator

The trajectory planning represents a crucial aspect of controlling serial manipulators in robotics. It involves generating smooth, collision-free and efficient paths for the robot's end-effector to accomplish various tasks.

Regarding trajectory planning for a serial manipulator, two main types are defined, the first is planned in the space of each joint, and the second in the Cartesian system, as observed in the specialized papers [10], [11], [12]. In this study, a joint space trajectory is used, the planned motion being carried out by the quartic polynomial interpolation method and defined on a simple case of start-move-stop. This trajectory is defined by point-to-point motion, as presented in the referenced paper [13]. Using quartic polynomial interpolation for joint space trajectory planning is a valid and widely used method, and it can be effectively applied to generate smooth and precise motions for 6-DoF serial manipulators.

In this context, the joint angles, joint angular velocities and joint angular accelerations have the following forms

$$\theta(t) = a_4 t^4 + a_3 t^3 + a_2 t^2 + a_1 t + a_0 \tag{30}$$

$$\dot{\theta}(t) = 4a_4 t^3 + 3a_3 t^2 + 2a_2 t + a_1 \tag{31}$$

$$\ddot{\theta}(t) = 12a_4 t^2 + 6a_3 t + 2a_2 \tag{32}$$

The initial conditions are the following

$$\begin{aligned}
&\theta(t_0) = \theta_0 \\
&\theta(t_f) = \theta_f \\
&\dot{\theta}(t_0) = C_1; \ddot{\theta}(t_0) = C_2; \dot{\theta}(t_f) = \ddot{\theta}(t_f) = 0
\end{aligned} \tag{33}$$

Considering the above, it is obtained

$$\begin{aligned}
a_0 &= \theta_0 \\
a_1 &= C_1 \\
a_2 &= \frac{C_2}{2} \\
a_3 &= \frac{4(\theta_f - \theta_0)}{t_f^3} - \frac{3C_1}{t_f^2} - \frac{2C_2}{t_f} \\
a_4 &= \frac{-3(\theta_f - \theta_0)}{t_f^4} + \frac{2C_1}{t_f^3} + \frac{C_2}{t_f^2}
\end{aligned} \tag{34}$$

where C_1 and C_2 represent values that are chosen based on the data of the problem.

5. Results

This case study considered the mathematical modeling and kinematic analysis of an ABB IRB7600 robotic arm. It was mathematically modeled using the Denavit-Hartenberg parameters, the forward and inverse kinematics solutions being generated and implemented using Matlab software. In this developed software the motion kinematics were tested and the relevant motion was determined.

Inverse kinematics of a robotic arm is used to determine the joint variables that control the motion of each joint in a robotic arm. This makes it possible to command the end effector of the robot to achieve the desired position and orientation in space.

For the imposed data of robotic arm angles, respectively $\theta_1 = 45^\circ, \theta_2 = 30^\circ, \theta_3 = 30^\circ, \theta_4 = -45^\circ, \theta_5 = 30^\circ, \theta_6 = 0^\circ$, the position of the final effector is determined by using direct kinematics, following the steps from subchapter 2.1, obtaining

$$[T]_6^0 = \begin{bmatrix} -0.5227 & 0.7500 & -0.4053 & 0.2586 \\ 0.3433 & -0.2500 & -0.9053 & 0.1336 \\ -0.7803 & -0.6124 & -0.1268 & -0.4601 \\ 0 & 0 & 0 & 1 \end{bmatrix} \tag{35}$$

Position of the end effector

$$\left\{P_6^0\right\} = \begin{Bmatrix} 0.2586 \\ 0.1336 \\ -0.4601 \end{Bmatrix} \tag{36}$$

The orientation of the end effector is given by the rotation matrix

$$\left[R\right]_6^0 = \begin{bmatrix} -0.5227 & 0.7500 & -0.4053 \\ 0.3433 & -0.2500 & -0.9053 \\ -0.7803 & -0.6124 & -0.1268 \end{bmatrix} \tag{37}$$

This case study considers the verification of the obtained data in terms of both forward and inverse kinematics.

For verifying angular relationships through inverse kinematics, considering the position and orientation of the end effector, the relationships obtained in Chapter 2.2 are taken into account. Thus, the position and orientation of the end effector from equations (36) and (37) are used, and the values of the angles for each joint are determined using the inverse kinematics model from equations (8)-(11), (21), (29), obtaining

Table 2

Joint angles obtained by applying the inverse kinematics model

$\theta_1 = 45^\circ$	$\theta_2 = 29.9977^\circ$	$\theta_3 = 29.9993^\circ$	$\theta_4 = -44.9962^\circ$	$\theta_5 = 30.0036^\circ$	$\theta_6 = -0.0052^\circ$

As observed, the obtained values of each joint angle through the inverse kinematics model are the same as the initial data from the forward kinematics model, leading to the validation of the presented model.

For the case where the polynomial trajectory described previously is used, the initial and final joint angles values are as follows

Table 3

Joint angles values

Joint angles [deg]	θ_1	θ_2	θ_3	θ_4	θ_5	θ_6
Start (Initial)	20	10	10	10	20	10
Stop (Final)	50	90	120	80	60	100

When considering the trajectory determination, based on the kinematic model of the ABB7600 robot, two simulation scenarios are taken into account. The first scenario assumes both initial and final velocities and accelerations to be zero, while the second scenario considers a non-zero initial velocity. The simulations for the two cases described above were conducted using the Matlab simulation environment.

The parametric relations for the end-effector trajectory in the first and second cases are as follows

$$\begin{aligned} x(t) &= c_1(0.41+1.075c_2+0.165c_{23}-1.056s_{23}-0.25c_5s_{23}-0.25c_{23}c_4s_5)-0.25s_1s_4s_5[m] \\ y(t) &= s_1(0.41+1.075c_2+0.165c_{23}-1.056s_{23}-0.25c_5s_{23}-0.25c_{23}c_4s_5)+0.25c_1s_4s_5[m] \\ z(t) &= 0.78-1.075s_2-0.165s_{23}-1.056c_{23}-0.25c_5c_{23}+0.25s_{23}c_4s_5[m] \end{aligned} \tag{38}$$

in which the following notations were

made $s_i = \sin\theta_i(t); c_i = \cos\theta_i(t); s_{ij} = \sin(\theta_i(t)+\theta_j(t)); c_{ij} = \cos(\theta_i(t)+\theta_j(t))$,

$i = j = \overline{1,6}$.

For each angular displacement, it was determined based on the first equation in system (39) for the first simulation case and the first equation in system (40) for the second simulation case.

The end-effector trajectory of the ABB7600 robot in the first simulation case ($C_1 = 0\,\text{deg}/s$; $C_2 = 0\,\text{deg}/s^2$) is shown in Fig.4.

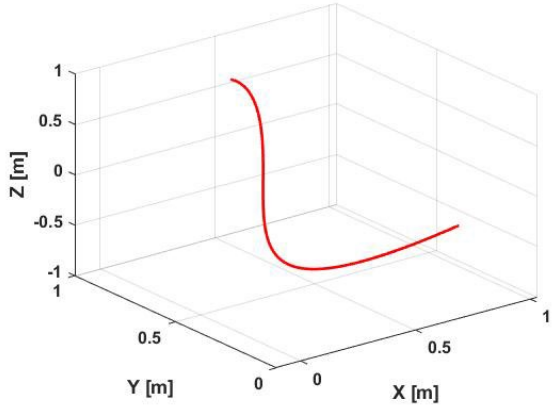

Fig. 4 End-effector trajectory in the first case

The results of the joint angles, joint angular velocities and joint angular accelerations in the first case of simulation are as shown on figures 5 to 7. The relationships of angular joints, angular velocities and angular accelerations in the first simulation case are as follows

$$\theta_i(t) = \theta_{0_i} + \frac{4(\theta_{f_i} - \theta_{0_i})}{t_f^3} t^3 - \frac{3(\theta_{f_i} - \theta_{0_i})}{t_f^4} t^4$$
$$\dot{\theta}_i(t) = \frac{12(\theta_{f_i} - \theta_{0_i})}{t_f^3} t^2 - \frac{12(\theta_{f_i} - \theta_{0_i})}{t_f^4} t^3 \quad (39)$$
$$\ddot{\theta}_i(t) = \frac{24(\theta_{f_i} - \theta_{0_i})}{t_f^3} t - \frac{36(\theta_{f_i} - \theta_{0_i})}{t_f^4} t^2$$

where $i = \overline{1,6}$, θ_{0_i} represents the initial joint angle, θ_{f_i} represents the final joint angle, both presented in Table 3, t_f represents the final time (in this case is 50s) and t represents the time for the entire simulation.

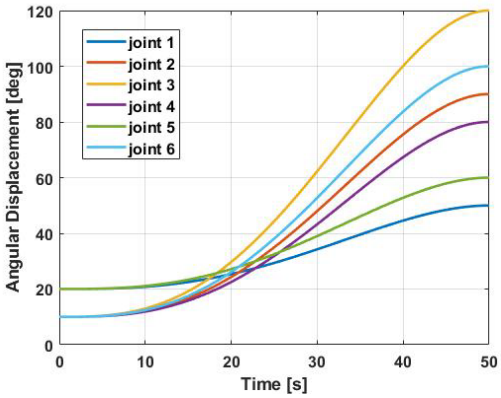

Fig. 5 Joint angles in the first case

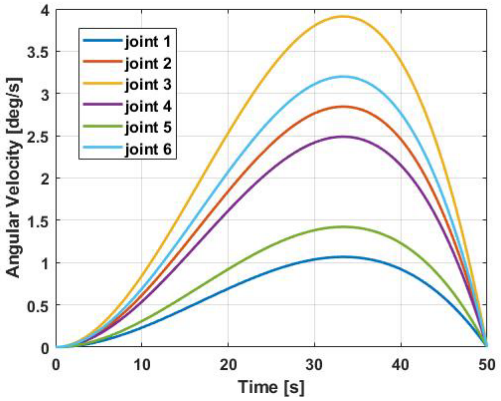

Fig. 6 Joint angular velocities in the first case

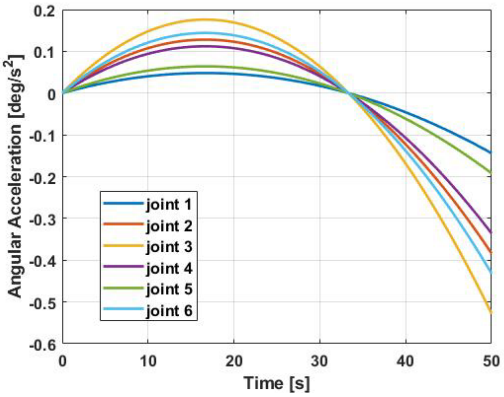

Fig. 7 Joint angular accelerations in the first case

Regarding the second simulation case ($C_1 = 1.5\,\text{deg}/s$; $C_2 = 0\,\text{deg}/s^2$), the end-effector trajectory is shown in Fig.8.

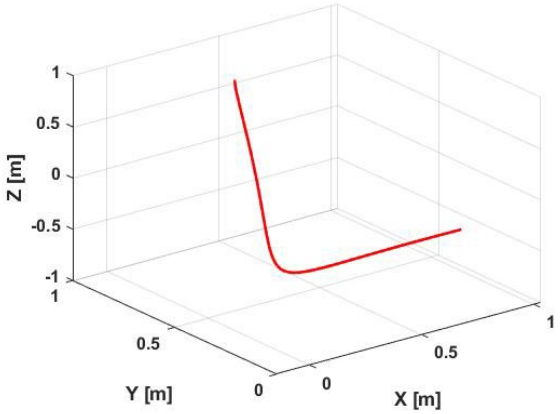

Fig. 8 End-effector trajectory in the second case

The results of the joint angles, joint angular velocities and joint angular accelerations in the second case of simulation are as shown on figures 9 to 11. The parametric equations in the first simulation case are as follows

$$\begin{aligned}\theta_i(t) &= \theta_{0_i} + \frac{4(\theta_{f_i}-\theta_{0_i})}{t_f^3}t^3 - \frac{3(\theta_{f_i}-\theta_{0_i})}{t_f^4}t^4 + 1.5t \\ \dot{\theta}_i(t) &= \frac{12(\theta_{f_i}-\theta_{0_i})}{t_f^3}t^2 - \frac{12(\theta_{f_i}-\theta_{0_i})}{t_f^4}t^3 + 1.5 \\ \ddot{\theta}_i(t) &= \frac{24(\theta_{f_i}-\theta_{0_i})}{t_f^3}t - \frac{36(\theta_{f_i}-\theta_{0_i})}{t_f^4}t^2\end{aligned} \tag{40}$$

where $i=\overline{1,6}$, θ_{0_i} represents the initial joint angle, θ_{f_i} represents the final joint angle, both presented in Table 3, t_f represents the final time (in this case is 50s) and t represents the time for the entire simulation.

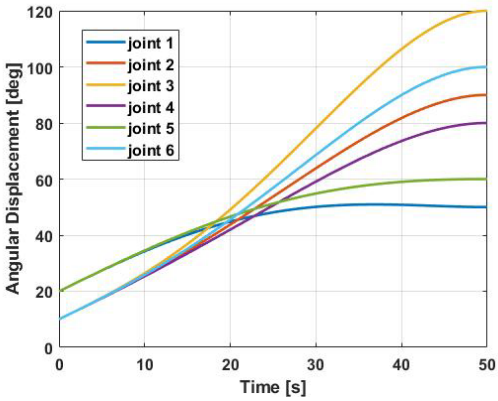

Fig. 9 Joint angles in the second case

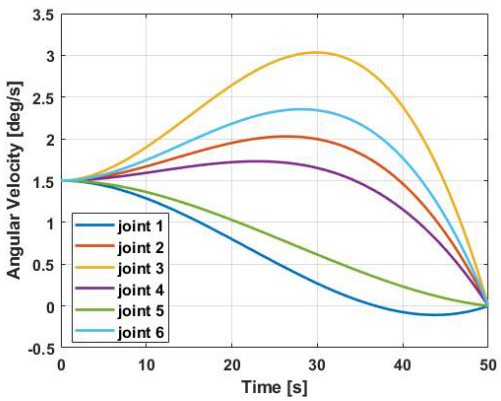

Fig. 10 Joint angular velocities in the second case

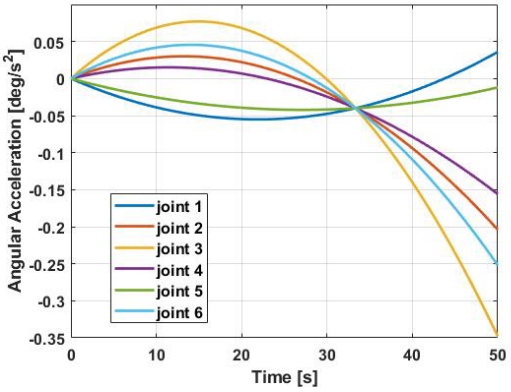

Fig. 11 Joint angular accelerations in the second case

As observed in Fig. 4 and Fig. 8, there are significant differences between the obtained end-effector trajectories are significant due to the modification of the initial velocity value. It is important to note that the simulation time was fixed at 50s for both cases. Due to the variations in velocity and acceleration between the two trajectories, energy consumption and the demand on the robot's motors may vary, as the aim is to reach the final position. A trajectory with zero initial and final acceleration will impose lower demands on the motors, whereas a trajectory with an imposed initial velocity may push the motors to their maximum capacity.

Analyzing Fig. 9, the effect of changing the velocity resulted in obtaining maximum angular displacements of approximately 5.5 degrees after 20 sec, while in the first simulation case, Fig. 5, the angular displacements remain unchanged during the motion. Regarding the angular velocities, in the first simulation case (Fig. 6), after approximately 34 sec, all joints reached their respective maximum values. On the other hand, in the second case (Fig. 10), after 30 sec, the first 4 joints reached their respective maximum values, while joints 5 and 6 showed a descending variation. The obtained results of angular acceleration depend largely on the results obtained for angular velocities. In the first simulation case (Fig. 7), when the angular velocity reaches its maximum value for all six joints, the angular acceleration becomes equal to zero. As observed in Fig. 11, the dependence of angular acceleration follows the same pattern as in Fig. 10, such that when the angular velocity reaches its maximum or minimum values, the acceleration becomes zero.

Since the aim is to achieve a smooth and shock-free motion, choosing the quartic interpolation method leads to minimizing the variation in acceleration. This study lays the theoretical groundwork for an experimental simulation to verify the validity of the results obtained and ensure they stay within acceptable limits, taking into account the algorithms presented in the specialized papers [14], [15], [16]. The experimental analysis, which will serve as the analysis for landing

at a fixed point on a mobile platform, will be carried out in the SpaceSysLab Maneciu Laboratory of the National Institute for Aerospace Research “Elie Carafoli”.

Fig. 12 INCAS ABB 7600 robotic arm

4. Conclusions

This article introduces the development of a kinematic model for a six-degree-of-freedom serial manipulator, and its simulations were conducted using Matlab simulation environments. The direct kinematics of the robot where studied by employing Denavit-Hartenberg parameters, while the inverse kinematics were achieved through an iterative calculation procedure. The main objective was to derive a mathematical model for the inverse kinematics of a six-degree-of-freedom serial manipulator, taking into account all relevant constraints on the variables.

Future advancements focus on enhancing the control of the serial manipulator's end effector, particularly when working with flexible elements, relying on the kinematic model presented in this research. Additionally, a trajectory of the end effector was established, and the variations in the six joint angles were carefully observed.

REFERENCES

[1]. *John J. Craig*, Introduction to Robotics. Mechanics and Control. Third edition, Pearson Prentice, United States of America, 2005.

[2]. *Zehranur Yilmaz, Orkun Yilmaz, Zafer Bingül*, Design, Analysis and Simulation of a 6-DOF Serial Manipulator, Kocaeli Journal of Science and Engineering, May 2020.

[3]. *Muhammad Bilal, Muhammad Osama Khan, Awais Mughal, Noman Ali*, Design and Control of 6 DOF Robotic Manipulator, Thesis for the degree of B.Sc. Mechatronics & Control Engineering, University of Engineering and Technology Lahore Faisalabad Campus, May 2018.
[4]. *Semaal Asif, Philip Webb*, Kinematics Analysis of 6-Dof Articulated Robot with Spherical Wrist, Mathematical Problems in Engineering, Hindawi, Vol 2021.
[5]. *Anastasia Tegopoulou, Evangelos Papadopoulos*, Determination of Rigid-Body Pose from Imprecise Point Position Measurements, IEEE/RSJ International Conference on Intelligent Robots and Systems, September 25-30, 2011, San Francisco, USA.
[6]. *ABB*, Operating manual RobotStudio, Sweden, 2008-2010.
[7]. *I. A. Vasilyev, A.M. Lyashin*, Analytical Solution to Inverse Kinematics Problem for 6-DOF Robot-Manipulator, Automation and Remote Control, p. 2195-2199, 2010.
[8]. *Serdar Küçük, Zafer Bingül*, The Inverse Kinematics Solutions of Industrial Robot Manipulators, Kocaeli University, July 2014.
[9]. *Mustafa Jabbar Hayawi*, The Closed Form Solution of the Inverse Kinematics of a 6-DOF Robot, Computer Science Department, Education College, Thi-Qar University, 2013.
[10]. *Marc Toussaint*, Robot Trajectory Optimization using Approximate Inference, 26th International Conference on Machine Learning , Montreal, Canada, 2009.
[11]. *A. Seddaoui, C.M. Saaj*, Optimised Collision-Free Trajectory and Controller Design for Robotic Manipulators, University of Surrey, February 2019.
[12]. *Prafull Kumar Tembhare, Ashish Kumar Khandelwal*, Trajectory Planning of 6 DOF Articulated Robotic Arm for Loading and Unloading Operations, Journal of Harmonized Research in Engineering, 2015.
[13]. *Mark W. Spong, Seth Hutchinson, M. Vidyasagar*, Robot Dynamics and Control, Second Edition, January 2004.
[14]. *Jian Zhang*, AI based Algorithms of Path Planning, Navigation and Control for Mobile Ground Robots and UAVs, October 2021.
[15]. *P.E. Teleweck, B. Chandrasekaran*, Path Planning Algorithms and Their Use in Robotic Navigation Systems, Journal of Physics Conference Series, April 2019.
[16]. *Francisco Rubio, Francisco Valero and Carlos Llopis-Albert*, A review of mobile robots: Concepts, methods, theoretical framework, and applications, International Journal of Advanced Robotic Systems, March-April 2019.